Technical Note

Institution of MECHANICAL ENGINEERS
Journal of AEROSPACE ENGINEERING

Proc IMechE Part G:
J Aerospace Engineering
2022, Vol. 236(13) 2842–2848

DOI: 10.1177/09544100211068218
journals.sagepub.com/home/pig
SAGE

Removing adverse effect of measurement process in flotation method

Rui Zhu[1,2], Qingguo Fei[1] and Dong Jiang[3]

Abstract

Ground simulation of space quasi-zero gravity environment is essential in modal testing of space structures. The air flotation method is widely used, in which the air cushion unit is attached to the measured structure. This inevitably increases the total mass of the structure to be tested and leads to the incorrect prediction of modal parameters. And irregular airflow disturbances of the air cushion unit also have negative effects on the test. The fast elimination method is presented to remove the adverse impact in the test data based on measured frequency response functions. Numerical simulations are performed employing the magnetometer structure. Results show that this method effectively removes the adverse mass and the airflow effect.

Keywords

Ground simulation, flotation method, airflow disturbances, elimination, frequency response function

Date received: 25 January 2021; revised: 29 September 2021; accepted: 9 November 2021

Introduction

Simulating the quasi-zero gravity environment of space is essential in the vibration test of aerospace structures.[1,2] The research and application of simulating space micro-low gravity environment on the ground have a long history and many research results. For example, the United States,[3] the Soviet Union, and other countries[4] have designed various micro-low gravity simulation systems for lunar rovers, astronauts, and other applications since the 1960s. According to different simulation principles, it can be divided into the air flotation method,[5,6] water flotation method,[7] drop testing tower method,[8,9] suspension method,[10,11] parabolic flight method,[12,13] and so on. The comparison of these methods[14] is shown in Table 1.

The air flotation method is widely used because of its low friction, high stability, long life, and many other advantages. This method is widely used for general spacecraft and robotics control simulations,[1] and applications are typical in vibration and deployment testing.[15] The influence of gravity in the ground environment can be counteracted by using the air cushion unit. Unlike the suspension method, the air flotation requires the air cushion unit attached to the measured structure. This method inevitably increases the total mass of the mock-up itself and leads to the incorrect prediction of modal parameters. Meanwhile, irregular airflow disturbances of the air cushion unit apply additional excitation on the structure. Two disadvantages above should be removed to improve measurement accuracy in the flotation method. The elimination problem can be transformed as the structure's modification, and an approach[16] is developed for reanalyzing a system with parameter perturbation using the measured frequency response functions (FRFs). In shaker modal testing, Bi et al.[17] eliminated the mass effects of the force transducer and accelerometer from point FRF and transfer FRF in the shaker test. Comparative experiments were investigated: (1) shaker + laser doppler vibrometer case and (2) shaker + accelerometer case. Zamani et al.[18] used sensitivity analysis to eliminate the mass effect, and the change in natural frequency was obtained according to the uncertainty in measuring frequency and resolution. To remove the additional mass in the modal test, Zhu et al.[19] investigated a hierarchical multi-transducers elimination method by successive application of the Sherman–Morrison theory. Based on the Sherman–Morrison–Woodbury (SMW) formula,[20] a one-step elimination method is proposed in Ref. 21. The distinct feature of this method is that it can eliminate the additional mass

[1] Institute of Aerospace Machinery and Dynamics, Southeast University, Nanjing, China
[2] Institute of Flight System Dynamics, Technical University of Munich, Munich, Germany
[3] School of Mechanical and Electronic Engineering, Nanjing Forestry University, Nanjing, China

Corresponding author:
Qingguo Fei, Institute of Aerospace Machinery and Dynamics, Southeast University, Nanjing, Jiangsu Province 211189, China.
Email: qgfei@seu.edu.cn

loading effects straightforwardly by one step, where the multiple masses are considered as multiple-element changes in the dynamic stiffness matrix. This is an approximate method to deal with the problems in the modal test using the flotation method.

In summary, most of the existing research studies focused on eliminating mass effects in the modal test. In contrast, limited attention has been focused on the adverse mass and the airflow effect in the air flotation method. Based on my previous work,[21] the elimination method is extended to the flotation method, where the mass of the air cushion should be removed as the attachment mass. Meanwhile, irregular airflow disturbances of the air cushion also are investigated. The air flotation method is introduced in the section Elimination Theory of Additional Influences. The elimination theory of additional influences in air flotation is presented in the section Elimination of Air Cushion Mass. The robustness of the method is analyzed with airflow distribution in the section Considering the Effect of Airflow Disturbance.

Elimination theory of additional influences

Modal testing using the air flotation method

The principle of the air flotation method is that the air is compressed into the air chamber of the air cushion unit. The compressed air is ejected at high speed through the throttle orifices and discharge grooves on the air chamber cover, thus forming an air cushion to support the magnetometer between the air cushion unit and the air flotation platform. Since the air layer between the surface and the mock-up is very thin (0.01 mm), the table's smoothness is high. Also, the surface material should not be deformed by temperature variations and gravity. The air flotation platform is made of granite to satisfy this requirement.[22] Air cushions are a sort of fluid cushion that uses compressed air as the lubrication medium.

As shown in Figure 1, the magnetometer is deployed on the flotation platform, and the bar is parallel to the air flotation platform. The primary deployment mechanism at the connecting frame's root is fixed by the transfer tooling and the modal test tooling. The magnetometer is supported on the flotation platform through the air cushion assembly.

As shown in Figure 2, the gravitational force of each air cushion is $\boldsymbol{S}_i$, and the subscript i indicates the number of air cushions. The measured structure (magnetometer) weight is $\boldsymbol{W}$. The mass of each air cushion is m_a. Each air cushion is pumped down to create buoyancy $\boldsymbol{T}_i$. Gravity can be compensated as follows

$$\boldsymbol{T}_1 + \boldsymbol{T}_2 + \boldsymbol{T}_3 + \boldsymbol{T}_4 = \boldsymbol{S}_1 + \boldsymbol{S}_2 + \boldsymbol{S}_3 + \boldsymbol{S}_4 + 4m_a + \boldsymbol{W} \tag{1}$$

Elimination of air cushion mass

As known, the flotation method can counteract the influence of gravity in the ground environment. The tested specimen (magnetometer) and the air cushion form the actual measured structure. The mass of the air cushion is inevitably added as the adverse condition in the test, which leads to the frequency reduction of the system. The elimination method is briefly introduced.

In the modal test, the method of force-hammer excitation is adopted. The geometric parameters of the magnetometer are introduced. In Figure 1, the mass of the magnetometer is 3.391 kg, the length is 4.8 m, and the mass of each air cushion is 0.1 kg. The corresponding finite element model is established in Nastran. Considering separately whether there is the mass of the air cushion or not; the related FRFs can be obtained through software analysis. The FRFs of the magnetometer without the air cushion are regarded as the exact value. The FRFs of the magnetometer with the air cushion are regarded as the measured value, which is not accurate due to the mass of the air cushion. Measured FRFs $\boldsymbol{h}^*$ with the air cushion's mass can be expressed as

$$\boldsymbol{h}^* = \begin{bmatrix} h_{11} & h_{12} & h_{13} & h_{14} \\ h_{21} & h_{22} & h_{23} & h_{24} \\ h_{31} & h_{32} & h_{33} & h_{34} \\ h_{41} & h_{42} & h_{43} & h_{44} \end{bmatrix} \tag{2}$$

Take driving point FRF h_{33} as an example. The exact and measured FRFs h_{33} are shown in Figure 3. Due to the air cushion attached in the magnetometer, the resonance frequencies of the system are lower than those of exact values.

The dynamic stiffness matrix $\boldsymbol{Z}$ of the measured system with the air cushion is expressed as

$$\boldsymbol{Z} = \boldsymbol{K} - \omega^2 \boldsymbol{M} + j\omega \boldsymbol{C} \tag{3}$$

where $\boldsymbol{M}$ is the mass matrix, $\boldsymbol{C}$ is the damping matrix, and $\boldsymbol{K}$ is the stiffness matrix.

The mass of air cushion m_a is regarded as the lumped mass, which is added in the magnetometer. The modification matrix $\Delta\boldsymbol{M}$ can be expressed as

$$\Delta\boldsymbol{M} = \begin{bmatrix} m_a & & & \\ & m_a & & \\ & & m_a & \\ & & & m_a \end{bmatrix} \tag{4}$$

The corresponding of dynamic stiffness matrix $\boldsymbol{Z}^*$ is written as

$$\boldsymbol{Z}^* = \boldsymbol{K} - \omega^2(\boldsymbol{M} + \Delta\boldsymbol{M}) + j\omega\boldsymbol{C} = \boldsymbol{Z} - \Delta\boldsymbol{Z} \tag{5}$$

where $\Delta\boldsymbol{Z}$ is expressed as

Table 1. Comparison of various micro-low gravity simulation methods.

Methods	Principe	Object	Type	Authenticity	Simulation time	Degree of freedom	Implementation difficulty	Advantages	Shortcoming
Air flotation	Air flotation support	Solar panel, deployment antenna and space manipulator	Micro-gravity	Higher	Infinite time	1–3	Easy	Simple implementation, adjustable force and unlimited time and size	Large additional mass and inertia and few adaptive degrees of freedom
Water flotation	Water flotation support	Large spacecraft and astronauts	Micro-gravity	Higher	Infinite time	6	Difficult	Unlimited time and size	Water resistance, sealing, and high cost
Drop testing tower	Free fall	Small spacecraft	Micro-gravity	High	10s	6	Difficult	Highest simulation accuracy	Shoot time, limited size, and high cost
Suspension	Sling suspension	Most spacecraft and astronauts	Micro-low gravity	High	Infinite time	3–6	Easy	Simple implementation, adjustable force, small additional inertia, and unlimited time and size	Complex control, unable to cross space, and easy to couple tremor for flexible body
Parabolic flight	Partial or complete free fall	Small spacecraft and astronauts	Micro-low gravity	High	20–30s	6	Hard	High simulation accuracy	Shoot time, limited size, and high cost

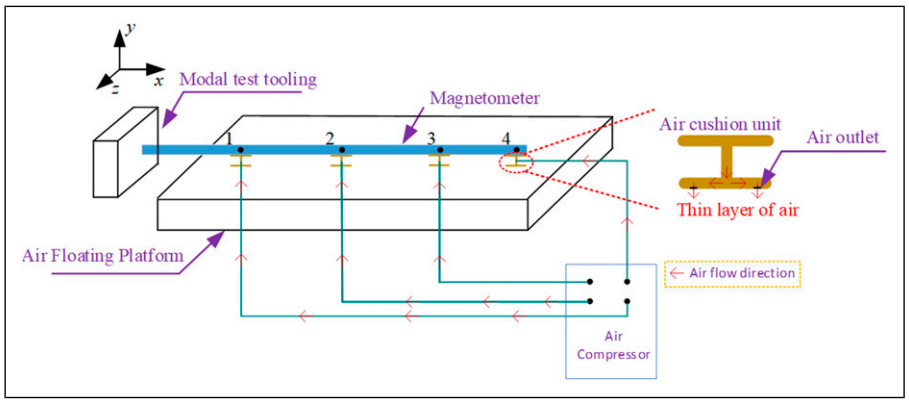

Figure 1. Schematic diagram of the modal test for the magnetometer on the flotation platform.

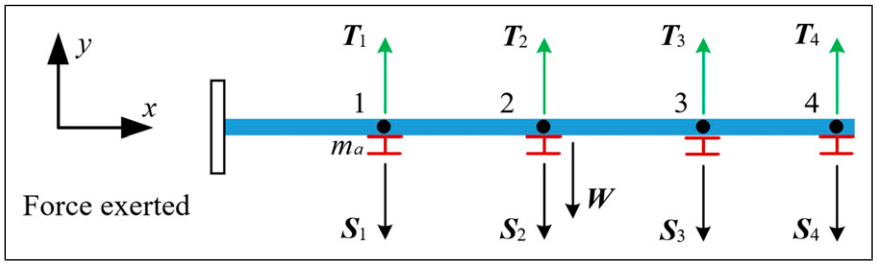

Figure 2. Force analysis in the vertical direction.

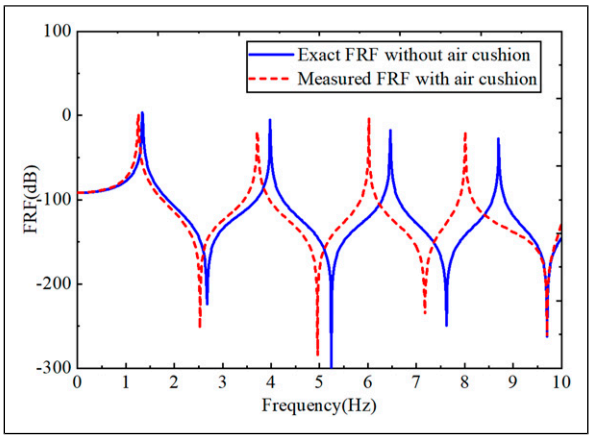

Figure 3. Comparison of exact and measured frequency response functions.

$$\Delta \boldsymbol{Z} = \begin{Bmatrix} 1 \\ 0 \\ 0 \\ 0 \end{Bmatrix} \begin{Bmatrix} \omega^2 m_a \\ 0 \\ 0 \\ 0 \end{Bmatrix}^T + \begin{Bmatrix} 0 \\ 1 \\ 0 \\ 0 \end{Bmatrix} \begin{Bmatrix} 0 \\ \omega^2 m_a \\ 0 \\ 0 \end{Bmatrix}^T + \begin{Bmatrix} 0 \\ 0 \\ 1 \\ 0 \end{Bmatrix} \begin{Bmatrix} 0 \\ 0 \\ \omega^2 m_a \\ 0 \end{Bmatrix}^T + \begin{Bmatrix} 0 \\ 0 \\ 0 \\ 1 \end{Bmatrix} \begin{Bmatrix} 0 \\ 0 \\ 0 \\ \omega^2 m_a \end{Bmatrix}^T \tag{6}$$

Equation (6) can be simplified as

$$\Delta \boldsymbol{Z} = \omega^2 \sum_{k=1}^{4} \boldsymbol{u}_k \boldsymbol{v}_k^T \tag{7}$$

where $\boldsymbol{u}_k$ and $\boldsymbol{v}_k$ are expressed as

$$\boldsymbol{u}_k = [0 \quad \cdots \quad 1_k \quad \cdots \quad 0]^T \tag{8}$$

$$\boldsymbol{v}_k = [0 \quad \cdots \quad (m_a)_k \quad \cdots \quad 0]^T \tag{9}$$

In $\boldsymbol{u}_k$ and $\boldsymbol{v}_k$, the subscript k indicates the location of the air cushion, which are 1 and m_a, respectively. Substituting equation (5) in (3), the dynamic stiffness matrix without transducers is obtained

$$\boldsymbol{Z} = \boldsymbol{Z}^* + \omega^2 \sum_{k=1}^{4} \boldsymbol{u}_k \boldsymbol{v}_k^T \tag{10}$$

Equation (10) is in the same form as the SMW, and one can obtain

$$\boldsymbol{Z}^{-1} = (\boldsymbol{Z}^*)^{-1} - \omega^2 (\boldsymbol{Z}^*)^{-1} [\boldsymbol{u}_1 \ \boldsymbol{u}_2 \ \boldsymbol{u}_3 \ \boldsymbol{u}_4] \boldsymbol{T}^{-1} \begin{bmatrix} \boldsymbol{v}_1^T \\ \boldsymbol{v}_2^T \\ \boldsymbol{v}_3^T \\ \boldsymbol{v}_4^T \end{bmatrix} (\boldsymbol{Z}^*)^{-1} \tag{11}$$

where $\boldsymbol{T}$ is a 4 × 4 matrix given by

According to the relationship between the dynamic stiffness matrix and the displacement FRF, we can obtain

$$\boldsymbol{T}=\begin{bmatrix} 1+\omega^2\boldsymbol{v}_1^T(\boldsymbol{Z}^*)^{-1}\boldsymbol{u}_1 & \omega^2\boldsymbol{v}_1^T(\boldsymbol{Z}^*)^{-1}\boldsymbol{u}_2 & \omega^2\boldsymbol{v}_1^T(\boldsymbol{Z}^*)^{-1}\boldsymbol{u}_3 & \omega^2\boldsymbol{v}_1^T(\boldsymbol{Z}^*)^{-1}\boldsymbol{u}_4 \\ \omega^2\boldsymbol{v}_2^T(\boldsymbol{Z}^*)^{-1}\boldsymbol{u}_1 & \omega^2\boldsymbol{v}_2^T(\boldsymbol{Z}^*)^{-1}\boldsymbol{u}_2 & \omega^2\boldsymbol{v}_2^T(\boldsymbol{Z}^*)^{-1}\boldsymbol{u}_3 & \omega^2\boldsymbol{v}_2^T(\boldsymbol{Z}^*)^{-1}\boldsymbol{u}_4 \\ \omega^2\boldsymbol{v}_3^T(\boldsymbol{Z}^*)^{-1}\boldsymbol{u}_1 & \omega^2\boldsymbol{v}_3^T(\boldsymbol{Z}^*)^{-1}\boldsymbol{u}_2 & \omega^2\boldsymbol{v}_3^T(\boldsymbol{Z}^*)^{-1}\boldsymbol{u}_3 & \omega^2\boldsymbol{v}_3^T(\boldsymbol{Z}^*)^{-1}\boldsymbol{u}_4 \\ \omega^2\boldsymbol{v}_4^T(\boldsymbol{Z}^*)^{-1}\boldsymbol{u}_1 & \omega^2\boldsymbol{v}_4^T(\boldsymbol{Z}^*)^{-1}\boldsymbol{u}_2 & \omega^2\boldsymbol{v}_4^T(\boldsymbol{Z}^*)^{-1}\boldsymbol{u}_3 & \omega^2\boldsymbol{v}_4^T(\boldsymbol{Z}^*)^{-1}\boldsymbol{u}_4 \end{bmatrix} \tag{12}$$

$$\boldsymbol{Z}^*=(\boldsymbol{h}^*)^{-1} \tag{13}$$

$$\boldsymbol{Z}=\boldsymbol{h}^{-1} \tag{14}$$

where $\boldsymbol{h}$ represents the displacement FRF of the initial system. So the corrected acceleration FRFs without the mass of the air cushion can be obtained by

$$\boldsymbol{h}=\boldsymbol{h}^*-\omega^2\boldsymbol{h}^*[\boldsymbol{u}_1 \quad \boldsymbol{u}_2 \quad \boldsymbol{u}_3 \quad \boldsymbol{u}_4]\boldsymbol{T}^{-1}\begin{bmatrix}\boldsymbol{v}_1^T\\ \boldsymbol{v}_2^T\\ \boldsymbol{v}_3^T\\ \boldsymbol{v}_4^T\end{bmatrix}\boldsymbol{h}^* \tag{15}$$

where the corresponding $\boldsymbol{T}$ is a 4 × 4 matrix given by

$$\boldsymbol{T}=\begin{bmatrix} 1+\omega^2\boldsymbol{v}_1^T\boldsymbol{h}^*\boldsymbol{u}_1 & \omega^2\boldsymbol{v}_1^T\boldsymbol{h}^*\boldsymbol{u}_2 & \omega^2\boldsymbol{v}_1^T\boldsymbol{h}^*\boldsymbol{u}_3 & \omega^2\boldsymbol{v}_1^T\boldsymbol{h}^*\boldsymbol{u}_4 \\ \omega^2\boldsymbol{v}_2^T\boldsymbol{h}^*\boldsymbol{u}_1 & \omega^2\boldsymbol{v}_2^T\boldsymbol{h}^*\boldsymbol{u}_2 & \omega^2\boldsymbol{v}_2^T\boldsymbol{h}^*\boldsymbol{u}_3 & \omega^2\boldsymbol{v}_2^T\boldsymbol{h}^*\boldsymbol{u}_4 \\ \omega^2\boldsymbol{v}_3^T\boldsymbol{h}^*\boldsymbol{u}_1 & \omega^2\boldsymbol{v}_3^T\boldsymbol{h}^*\boldsymbol{u}_2 & \omega^2\boldsymbol{v}_3^T\boldsymbol{h}^*\boldsymbol{u}_3 & \omega^2\boldsymbol{v}_3^T\boldsymbol{h}^*\boldsymbol{u}_4 \\ \omega^2\boldsymbol{v}_4^T\boldsymbol{h}^*\boldsymbol{u}_1 & \omega^2\boldsymbol{v}_4^T\boldsymbol{h}^*\boldsymbol{u}_2 & \omega^2\boldsymbol{v}_4^T\boldsymbol{h}^*\boldsymbol{u}_3 & \omega^2\boldsymbol{v}_4^T\boldsymbol{h}^*\boldsymbol{u}_4 \end{bmatrix} \tag{16}$$

In Figure 4, the corresponding corrected FRF h_{33} is compared to the exact FRF. Results show that the corrected FRF is in quite good agreement with the exact values.

It is a suitable way to assess the results by comparing the natural frequencies[23,24] of the exact, measured, and corrected FRFs. The natural frequencies are shown in Table 2. Due to the air cushion's attachment, the measured frequencies are lower than the exact values. The error of exact and measured frequency is shown in the fourth line. The maximum error occurs at the 3rd order frequency (5.56%), and the other errors are 4.58% (1st order) and 5.10% (2nd order). As expected, the proposed method successfully removes the mass of the air cushion.

Considering the effect of airflow disturbance

The robustness of the proposed method is analyzed. The air reaction counteracts the influence of gravity in the ground environment. Due to the airflow disturbances, the vibration response signals can be adversely contaminated. It is necessary to take into account the effect of the measuring error of FRFs. In Figure 5, the impact of the airflow disturbance is regarded as white noise.[25]

In the modal analysis, the frequency response function $\boldsymbol{H}(\omega)$ reflects the relationship between the input and output

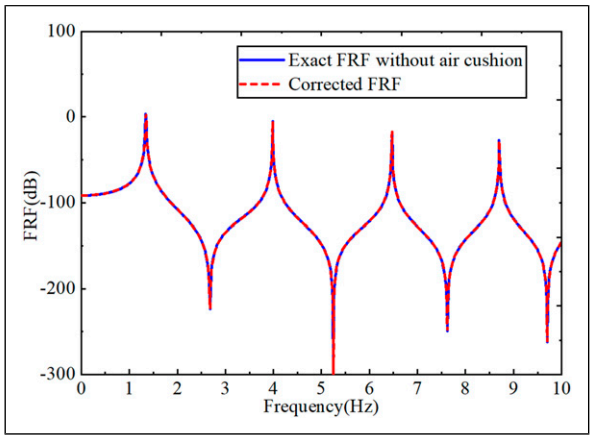

Figure 4. Comparison of exact and corrected frequency response functions.

of the system and represents the system's inherent characteristics as follows

$$\boldsymbol{H}(\omega)=\frac{\boldsymbol{X}(\omega)}{\boldsymbol{F}(\omega)} \tag{17}$$

where $\boldsymbol{F}(\omega)$ is the excitation input, and $\boldsymbol{X}(\omega)$ is the response output.

Considering the airflow disturbance, $\boldsymbol{F}(\omega)$ includes the impulse excitation $\boldsymbol{F}_{Impulse}$ and random input $\boldsymbol{F}_{Random}$ in hammering tests. The random input $\boldsymbol{F}_{\text{random}}$ is represented by

$$\boldsymbol{F}_{Random}=\boldsymbol{R}_1+\boldsymbol{R}_2+\boldsymbol{R}_3+\boldsymbol{R}_4 \tag{18}$$

where the random force of each air cushion in the horizontal direction is expressed as $\boldsymbol{R}_i$.

Equation (17) can be written as

$$\boldsymbol{H}_{Exact}=\frac{\boldsymbol{X}_{Measured}}{(\boldsymbol{F}_{Impulse}+\boldsymbol{F}_{Random})} \tag{19}$$

Then, the measured FRFs $\boldsymbol{H}_{Measurd}$ is obtained by

$$\begin{aligned}\boldsymbol{H}_{Measured}&=\frac{\boldsymbol{X}_{Measured}}{\boldsymbol{F}_{Impulse}}\\ &=\boldsymbol{H}_{Exact}\frac{(\boldsymbol{F}_{Impulse}+\boldsymbol{F}_{Random})}{\boldsymbol{F}_{Impulse}}\end{aligned} \tag{20}$$

As shown in equation (20), $\boldsymbol{H}_{Measurd}$ is equal to $\boldsymbol{H}_{Exact}$ without random input.

Table 2. Natural frequencies of the exact, measured, and corrected FRFs.

Mode order	1	2	3
Exact frequency (Hz)	0.262	1.644	4.606
Measured frequency (Hz)	0.250	1.564	4.350
Error of exact and measured frequency (%)	4.58	5.10	5.56
Corrected frequency (Hz)	0.262	1.644	4.606

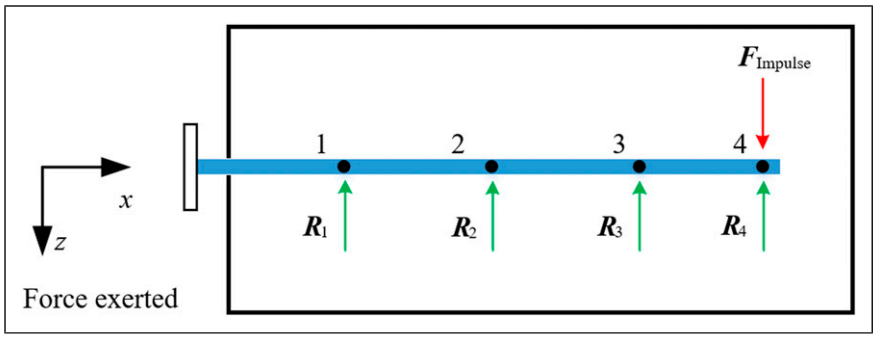

Figure 5. Force analysis with the airflow disturbance in the horizontal direction.

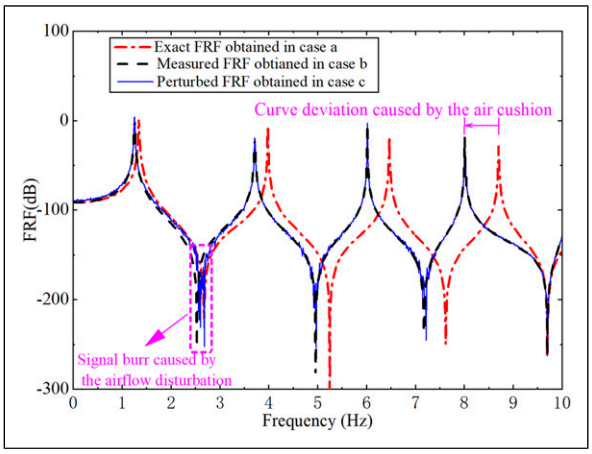

Figure 6. Comparison of frequency response functions obtained in three cases.

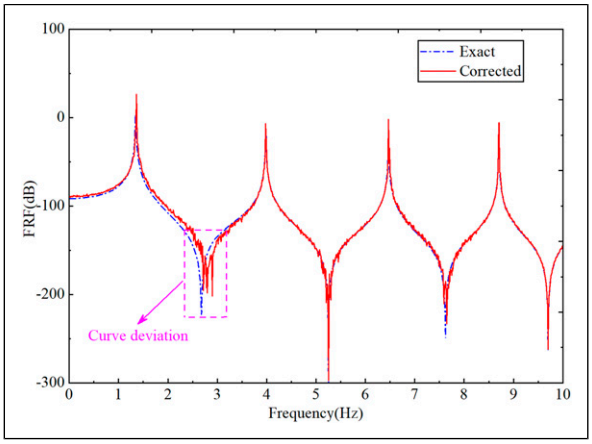

Figure 7. Comparison of corrected (including airflow disturbance) and exact frequency response functions.

Take driving point FRF h_{44} as an example, three cases are conducted. Case a: Without air cushion, the exact h_{44} is obtained by impulse excitation at coordinate 4; Case b: In the same exciting force, the measured h_{44} is obtained by impulse excitation at coordinate 4 with air cushion. Case c: Considering the effect of the airflow disturbance with the air cushion, the 5% white noise is excited at the displacement of the air cushion, and unit impulse excitation is added at coordinate 4. Then, the perturbed FRF h_{44} is obtained. As shown in Figure 6, the measured FRF shifts to the left compared with the exact FRF, where the natural frequencies of the measured FRF decrease. Meanwhile, the perturbed FRF has a signal burr due to the airflow distribution compared to the measured FRF h_{44}.

The proposed method is utilized to eliminate the mass of transducers with the airflow distribution. The corrected and exact FRF h_{44} are presented in Figure 7. Results showed that the proposed method successfully eliminates the multi-transducers mass loading effect, and the corrected FRFs match perfectly with the exact FRFs. The proposed method has robustness for the airflow distribution.

Conclusion

To simulating the quasi-zero gravity environment of space, the air flotation method is widely used. The mass of the air cushion unit and the airflow disturbance inevitably pollute the measured data, which affects the accuracy of modal identification. The elimination method is utilized to remove adverse effects by using the measured FRFs. The advantage of the presented method is that it can eliminate mass loading effects of air cushion units straightforwardly based on measured data in the air flotation method, which can improve the accuracy of modal identification. The

disadvantage of this method is that when the structure is complex and there are many air cushions arranged, the amount of frequency response function data required by this method is large, and a certain calculation time is required. After using the proposed method, the corrected FRFs from the measured data are in quite good agreement with the exact value. Besides, the proposed method has robustness for the airflow distribution in the flotation method, which is of great significance in aerospace engineering.

Declaration of conflicting interests

The author(s) declared no potential conflicts of interest with respect to the research, authorship, and/or publication of this article.

Funding

The author(s) disclosed receipt of the following financial support for the research, authorship, and/or publication of this article: This research work is supported by the National Natural Science Foundation of China (11602112, 11572086), Postgraduate Research & Practice Innovation Program of Jiangsu Province (KYCX19_0062), the Jiangsu Natural Science Foundation (BK20170022), and the Scientific Research Foundation of Graduate School of Southeast University.

ORCID iD

Rui Zhu https://orcid.org/0000-0001-8873-7098

References

1. Schwartz JL, Peck MA and Hall CD. Historical review of air-bearing spacecraft simulators. *J Guid Control Dyn* 2003; 26(4): 513–522.
2. Greschik G and Belvin WK. High-fidelity gravity offloading system for free-free vibration testing. *J Spacecr Rockets* 2007; 44(1): 132–142.
3. Wilson W, Jones L and Peck M. A multimodule planar air bearing testbed for cubesat-scale spacecraft. *ASME J Dyn Syst Meas Control* 2013; 135(4): 045001.
4. Christian S. Canadian space robotic activities. *Acta Astronaut* 1997; 41(10): 239–246.
5. SCHUBERT H. *How J P. Space Construction: An Experimental Testbed to Develop Enabling Technologies//Proceedings of SPIE - the International Society for Optical Engineering*. Pittsburgh, PA, United States: SPIE, 1997, pp. 179–188.
6. Rybus T and Seweryn K. Planar air-bearing microgravity simulators: review of applications, existing solutions and design parameters. *Acta Astronaut* 2016; 120: 239–259.
7. Laughlin M, Murry J, Lee L, et al. *Compiling a Comprehensive EVA Training Dataset for NASA Astronauts*, 2016.
8. Chen CI, Chen YT, Wu SC, et al. Experiment and simulation in design of the board-level drop testing tower apparatus. *Exp Tech* 2012; 36(2): 60–69.
9. Kufner E, Blum J, Callens N, et al. ESA's drop tower utilisation activities 2000 to 2011. *Microgravity Sci Technol* 2011; 23(4): 409–425.
10. Meguro A, Shintate K, Usui M, et al. In-orbit deployment characteristics of large deployable antenna reflector onboard Engineering Test Satellite VIII. *Acta Astronaut* 2009; 65(9–10): 1306–1316.
11. Santiago J and Baier H. Advances in deployable structures and surfaces for large apertures in space. *Ceas Space J* 2013; 5(3–4): 89–115.
12. Nicolau E, Poventud-Estrada CM, Arroyo L, et al. Microgravity effects on the electrochemical oxidation of ammonia: a parabolic flight experiment. *Electrochim Acta* 2012; 75: 88–93.
13. Block J, Bäger A, Behrens J, et al. A self-deploying and self-stabilizing helical antenna for small satellites. *Acta Astronaut* 2013; 86: 88–94.
14. Gao H, Niu F, Liu Z, et al. Suspended micro-low gravity environment simulation technology: status quo and prospect. *Acta Aeronaut et Astronaut Sin* 2021; 42(1): 523911 (In Chinese).
15. McEachen ME. Validation of slender lattice trusses by modeling and testing. *J Spacecr Rockets* 2012; 49(6): 970–977.
16. Özgüven HN. Structural modifications using frequency response functions. *Mech Syst Signal Process* 1990; 4(1): 53–63.
17. Bi S, Ren J, Wang W, et al. Elimination of transducer mass loading effects in shaker modal testing. *Mech Syst Signal Process* 2013; 38(2): 265–275.
18. Zamani P, Taleshi Anbouhi A, Ashory MR, et al. Cancelation of transducer effects from frequency response functions: experimental case study on the steel plate. *Adv Mech Eng* 2016; 8(4): 1–12.
19. Zhu R, Fei Q, Jiang D, et al. Using Sherman–Morrison theory to remove the coupled effects of multi-transducers in vibration test. *Proc Inst Mech Eng G J Aerosp Eng* 2019; 233(4): 1364–1376.
20. Zhu R, Fei Q-G, Jiang D, et al. Dynamic sensitivity analysis based on Sherman–Morrison–Woodbury formula. *AIAA J* 2019; 57(11): 4992–5001.
21. Zhu R, Fei Q, Jiang D, et al. Removing mass loading effects of multi-transducers using Sherman–Morrison–Woodbury formula in modal test. *Aerosp Sci Technol* 2019; 93: 105241.
22. Schlotterer M and Theil S. Testbed for on-orbit servicing and formation flying dynamics emulation. In: AIAA guidance, navigation, and control conference, Toronto, Canada, 2–5 August 2010.
23. Zhu R, Fei Q, Jiang D, et al. Identification of nonlinear stiffness and damping parameters using a hybrid approach. *AIAA J* 2021; 5: 1–10.
24. Zhu R, Fei Q, Jiang D, et al. Bayesian model selection in nonlinear subspace identification. *AIAA J* 2021; 8: 1–10.
25. Jia Y, Yang Z and Song Q. Experimental study of random dynamic loads identification based on weighted regularization method. *J Sound Vibr* 2015; 342: 113–123.

Appendix

Notation

$\boldsymbol{h}$ Frequency response function
$\boldsymbol{K}$ Stiffness matrix
$\boldsymbol{M}$ Mass matrix
m_a Mass of each air cushion
$\boldsymbol{R}_i$ Random force of each air cushion in the horizontal direction; i indicates the number of air cushions
$\boldsymbol{S}_i$ Gravitational force of every air cushion
$\boldsymbol{T}_i$ Buoyancy
$\boldsymbol{W}$ Weight of the structure
$\boldsymbol{X}$ Response output
$\boldsymbol{Z}$ Dynamic stiffness matrix
ω Angular frequency (rad/s)